

Photonic nanojet enhancement of backscattering of light by nanoparticles: a potential novel visible-light ultramicroscopy technique

Zhigang Chen and Allen Taflove

Department of Electrical and Computer Engineering, Northwestern University, Evanston, Illinois 60208
z-chen@northwestern.edu

Vadim Backman

Department of Biomedical Engineering, Northwestern University, Evanston, Illinois 60208

Abstract: We report what we believe to be the first evidence of localized nanoscale photonic jets generated at the shadow-side surfaces of micron-scale, circular dielectric cylinders illuminated by a plane wave. These photonic nanojets have waists smaller than the diffraction limit and propagate over several optical wavelengths without significant diffraction. We have found that such nanojets can enhance the backscattering of visible light by nanometer-scale dielectric particles located within the nanojets by several orders of magnitude. Not involving evanescent fields and not requiring mechanical scanning, photonic nanojets may provide a new means to detect and image nanoparticles of size well below the diffraction limit. This could yield a potential novel ultramicroscopy technique using visible light for detecting proteins, viral particles, and even single molecules; and monitoring molecular synthesis and aggregation processes of importance in many areas of biology, chemistry, material sciences, and tissue engineering.

© 2004 Optical Society of America

OCIS codes: (170.0170) Medical optics and biotechnology; (170.0180) Microscopy; (290.0290) Scattering; (290.1350) Backscattering.

References

1. D. W. Pohl, W. Denk, and M. Lanz, "Optical stethoscopy: Image recording with resolution $\lambda/20$," *Appl. Phys. Lett.* **44**, 651-653 (1984).
2. A. Lewis, M. Isaacson, A. Harootunian, and A. Muray, "Development of a 500Å resolution microscope," *Ultramicroscopy* **13**, 227-231 (1984).
3. E. Betzig, A. Lewis, A. Harootunian, M. Isaacson, and E. Kratschmer, "Near-field scanning optical microscopy (NSOM): Development and biophysical applications," *Biophys. J.* **49**, 269-279 (1986).
4. E. Betzig and J. K. Trautman, "Near-field optics: Microscopy, spectroscopy, and surface modification beyond the diffraction limit," *Science* **257**, 189-195 (1992).
5. B. Dunn, "Near-field scanning optical microscopy," *Chem. Rev.* **99**, 2891-2928 (1999).
6. S. M. Mansfield and G. S. Kino, "Solid immersion microscope," *Appl. Phys. Lett.* **57**, 2615-2616 (1990).
7. L. Novotny, E. J. Sanchez, and X. S. Xie, "Near-field optical imaging using metal tips illuminated by high-order Hermite-Gaussian beams," *Ultramicroscopy* **71**, 21-29 (1998).
8. E. J. Sanchez, L. Novotny, and X. S. Xie, "Near-field fluorescence microscopy based on two-photon excitation with metal tips," *Phys. Rev. Lett.* **82**, 4014-4017 (1999).
9. B. B. Goldberg, S. B. Ippolito, L. Novotny, Z. Liu, and M. S. Ünlü, "Immersion lens microscopy of photonic nanostructures and quantum dots," *IEEE J. Sel. Top. Quant. Elect.* **8**, 1051-1059 (2002).
10. A. Taflove and S. Hagness, *Computational Electrodynamics: The Finite-Difference Time-Domain Method* (Artech, Boston, MA, 2000).
11. J. F. Owen, R. K. Chang, and P. W. Barber, "Internal electric field distributions of a dielectric cylinder at resonance wavelengths," *Opt. Lett.* **6**, 540-542 (1981).
12. D. S. Benincasa, P. W. Barber, J.-Z. Zhang, W.-F. Hsieh, and R. K. Chang, "Spatial distribution of the internal and near-field intensities of large cylindrical and spherical scatters," *Appl. Opt.* **26**, 1348-1356 (1987).
13. C. L. Adler, J. A. Lock, B. R. Stone, and C. J. Garcia, "High-order interior caustics produced in scattering of a diagonally incident plane wave by a circular cylinder," *J. Opt. Soc. Am. A* **14**, 1305-1315 (1997).

14. J. A. Lock, C. L. Adler, and E. A. Hovenac, "Exterior caustics produced in scattering of a diagonally incident plane wave by a circular cylinder: semiclassical scattering theory analysis," *J. Opt. Soc. Am. A* **17**, 1846-1856 (2000).
 15. Z. Chen, A. Taflove, and V. Backman, "Equivalent volume-averaged light scattering behavior of randomly inhomogeneous dielectric spheres in the resonant range," *Opt. Lett.* **28**, 765-767 (2003).
 16. Z. Chen, A. Taflove, and V. Backman, "Concept of the equiphase sphere for light scattering by nonspherical dielectric particles," *J. Opt. Soc. Am. A* **21**, 88-97 (2004).
 17. C. F. Bohren and D. R. Huffman, *Absorption and Scattering of Light by Small Particles* (Wiley, New York, 1983).
 18. J.-P. Berenger, "A perfectly matched layer for the absorption of electromagnetic waves," *J. Comput. Phys.* **114**, 185-200 (1994).
-

1. Introduction

Optical microscopy and spectroscopy technologies are well established and are remarkably powerful. Critical to any discussion of them are the fundamental limitations of conventional microscopy. In the case of imaging objects with optical fields propagating in the far-field zone, the fundamental constraint is the diffraction of light which limits conventional optical microscopy to a spatial resolution comparable to one-half wavelength, or about 200 nm for visible light. As problems of interest push further into the nanometric regime, the importance of imaging techniques that allow nanoscale resolution or sensitivity has been steadily increasing.

Near-field optical techniques making use of the evanescent field have been developed to overcome the diffraction limit of far-field optics. In particular, a proximal-probe technique called near-field scanning optical microscopy (NSOM) has extended the range of optical measurements beyond the diffraction limit and stimulated interest in many disciplines, especially material and biological sciences [1-5]. However, the low light-collection efficiency, relatively slow image-acquisition rate, and incapability to image or sense objects below the surface of NSOM fundamentally limits its utility. An alternative to NSOM, solid immersion lens (SIL) microscopy [6], reduces the wavelength by immersing the object space in a material with a high refractive index. This improves resolution without a large loss of light. More recently, a tip-enhanced near-field optical microscopy technique has been developed [7-9]. This technique combines SIL microscopy with enhanced focusing caused by a strongly peaked electric field adjacent to a sharply pointed metal tip. With this technique, spectroscopic measurements having a spatial resolution of 10 nm have been achieved [8].

In this paper, we report what we believe to be the first evidence of localized photonic nanojets generated at the shadow-side surfaces of micron-scale, circular dielectric cylinders illuminated by a plane wave. Using high-resolution finite-difference time-domain (FDTD) numerical modeling [10], we have found that photonic nanojets have waists smaller than the diffraction limit and propagate over several optical wavelengths without significant diffraction. We have further found that such nanojets can enhance the backscattering of visible light by nanometer-scale dielectric particles located within the nanojets by several orders of magnitude. This may provide a new ultramicroscopy technique for using visible light to detect and image nanoparticles such as proteins, viral particles, and even single molecules; and monitoring molecular synthesis and aggregation processes of importance in many areas of biology, chemistry, material sciences, and tissue engineering.

2. Photonic nanojets

Several calculations have been reported for the spatial distributions of the internal and near-external electromagnetic fields of plane-wave-illuminated infinite circular dielectric cylinders [11-12]. These calculations have shown that high-intensity peaks can exist in both the internal and near-external fields along the incident axis even for nonresonant conditions. The location and the intensity of these near-field peaks depend upon the refractive index contrast between the cylinder and its surrounding medium, as well as the size parameter $x = ka = 2\pi a/\lambda$ of the cylinder (where a is the radius and λ is the incident wavelength)

[12]. More recently, interior and exterior caustics produced in the scattering of a diagonally incident plane wave by a circular cylinder have been examined using ray theory [13] and the semiclassical limit of electromagnetic wave scattering theory [14].

Using high-resolution FDTD numerical solutions of Maxwell's equations, we have revisited the phenomenology of the generation of peaks of the internal and near-external fields of a plane-wave-illuminated dielectric cylinder. Previously, the FDTD method has shown promise in calculating scattering by realistic particles because of its ability to model complex surface shapes and internal structures [10, 15, 16]. The two-dimensional (2-D) transverse magnetic (TM) case has been considered, i.e., wherein the incident magnetic field vector is perpendicular to the axis of an infinitely long cylinder of fixed cross section. Optical wavelengths of about 500 nm and cylinder diameters of about 5 μm have been investigated.

Our FDTD computer code was first verified by calculating the differential scattering cross section of several homogeneous, isotropic, circular dielectric cylinders and comparing these results to the exact solution based on the separation-of-variables method [17]. The perfectly matched layer (PML) absorbing boundary condition [18] was used in our FDTD simulations to efficiently terminate the outer boundary of the computational lattice. With the FDTD space lattice having a uniform square cell size of 1.25 nm (finer than 1/100th dielectric wavelength for all computer runs), the results for the scattering cross section agreed with the exact solution to within ± 1.5 dB over the entire range of scattering angles for all cases studied. Typical computational dynamic ranges for this level of agreement were 60 dB.

Having validated the FDTD numerical modeling procedure, we proceeded to study in detail the internal and near-external fields of a series of homogeneous, isotropic, circular dielectric cylinders. Figure 1 shows key results that illustrate the evolution of a photonic nanojet as the refractive index of the cylinder is changed relative to that of its surrounding medium. In this case, we consider an infinite dielectric circular cylinder of diameter $d = 5$ μm and refractive index n_1 embedded within an infinite vacuum medium of refractive index of $n_2 = 1.0$. The cylinder is normally illuminated by a rightward-propagating sinusoidal plane wave of wavelength $\lambda_2 = 500$ nm in medium 2. Figures 1(a), 1(b), and 1(c) visualize the FDTD-calculated envelope of the sinusoidal steady-state electric field for $n_1 = 3.5$, 2.5, and 1.7, respectively. With each decrease of n_1 , it is evident that the internal electric-field peak shifts toward the shadow-side surface of the cylinder along the forward direction. Finally, the electric-field peak emerges from the shadow-side surface of the cylinder in Fig. 1(c) as a strong jet-like distribution. The most striking feature of this photonic jet is that it is neither evanescent nor diffracting. It has a length of about 900 nm (slightly less than $2\lambda_2$) and a full width at half maximum (FWHM) waist of about 250 nm ($0.5\lambda_2$). In terms of intensity (defined as squared electric field) distribution, it has a waist of about 200 nm, smaller than one-half wavelength. The emergence of a photonic jet from the shadow-side surface of this dielectric cylinder for $n_1 \sim 2$ is primarily consistent with previous work on optical caustics generated by dielectric circular cylinders [13, 14]. For scattering of a normally incident plane wave, the position of the cusp point focal line of the interior cusp caustics generated by dielectric circular cylinders embedded within an infinite vacuum medium is given by [13]

$$f = a(-1)^p / (2p - 1 - n_1) \quad (1)$$

whereas the cusp point focal line of the exterior caustics consisting of a $p = 1$ near-zone cylindrical aberration cusp caustic is given by [13, 14]

$$f = an_1 / [2(n_1 - 1)] \quad (2)$$

where a is the radius of the cylinder, n_1 is the refractive index of the cylinder, and p denotes the number of internal chords of the ray trajectories, i.e., the family of rays that produces either an interior or exterior caustic has undergone $p-1$ internal reflections before the caustic is formed. Equations (1) and (2) may be used to approximately predict the position of the internal electric field peak and analyze the evolution of photonic jets.

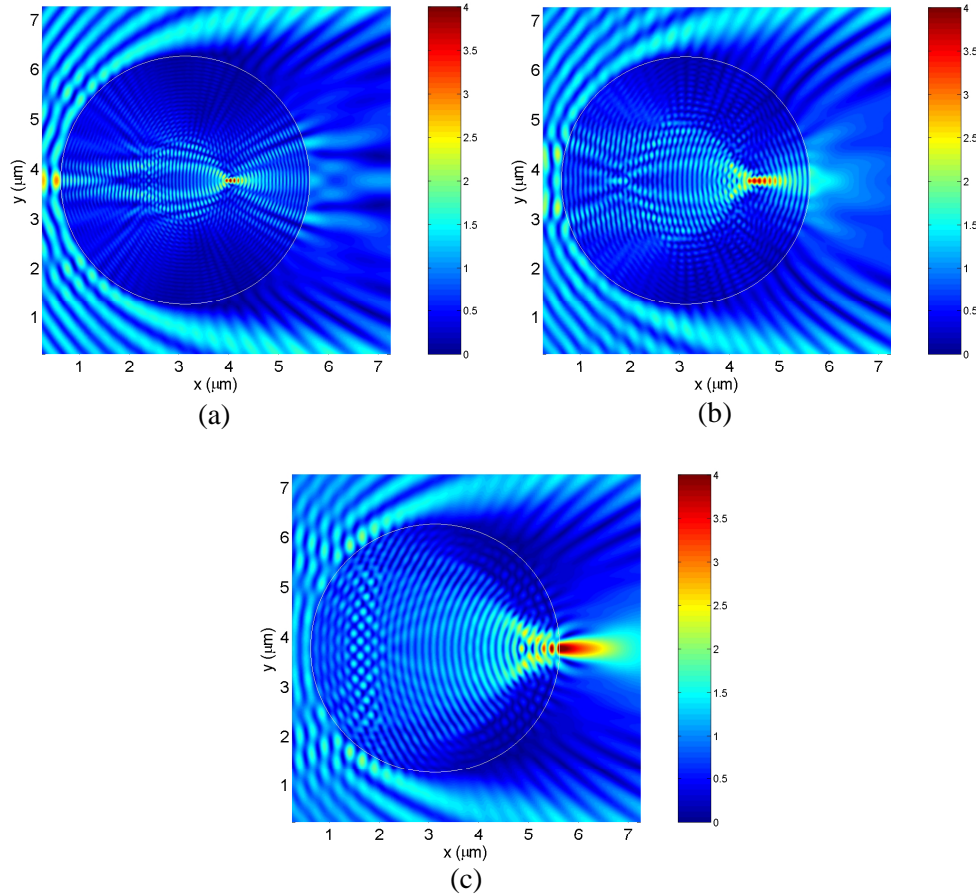


Fig. 1. Evolution of a photonic nanojet as the refractive index of a plane-wave-illuminated circular dielectric cylinder decreases. The FDTD-calculated envelope of the sinusoidal steady-state electric field is visualized for a $d = 5 \mu\text{m}$ circular cylinder of uniform refractive index n_1 embedded within an infinite vacuum medium of refractive index $n_2 = 1.0$. Light of wavelength $\lambda_2 = 500 \text{ nm}$ propagates from left to right in medium 2. (a) $n_1 = 3.5$; (b) $n_1 = 2.5$; (c) $n_1 = 1.7$.

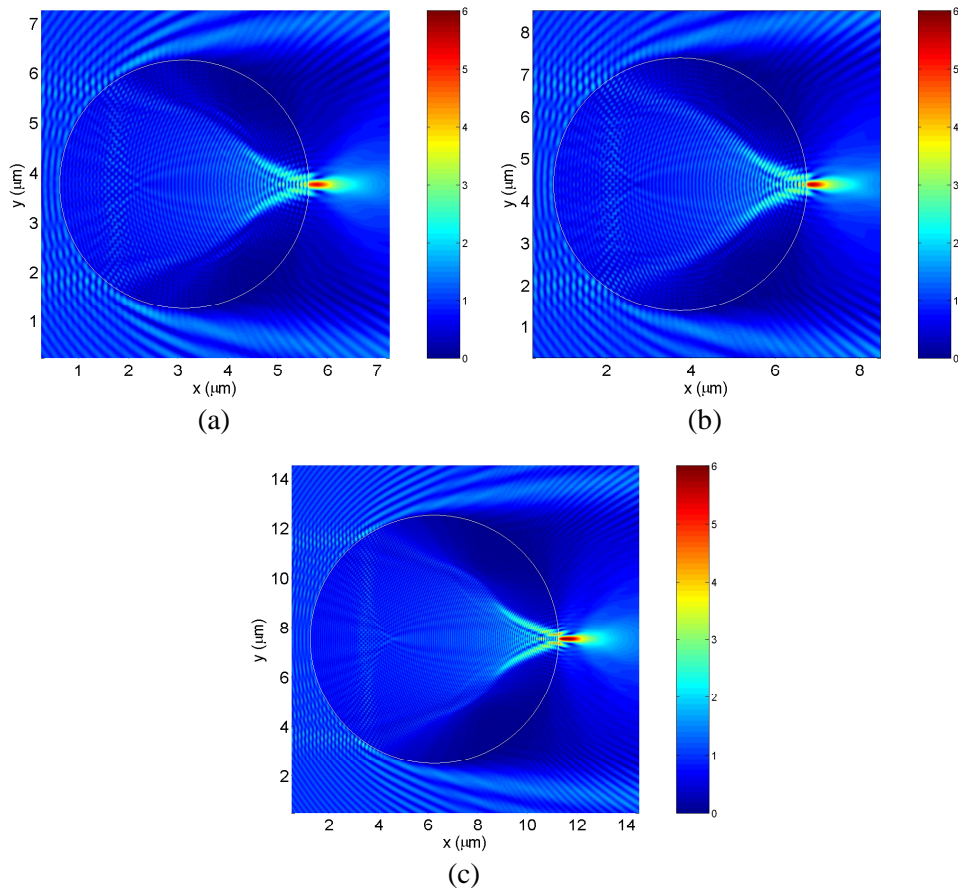


Fig. 2. Generation of photonic nanojets similar to that in Fig. 1(c) for three different combinations of d , n_1 , n_2 , and λ_2 : (a) $d = 5 \mu\text{m}$, $n_1 = 3.5$, $n_2 = 2.0$, $\lambda_2 = 250 \text{ nm}$; (b) $d = 6 \mu\text{m}$, $n_1 = 2.3275$, $n_2 = 1.33$, $\lambda_2 = 300 \text{ nm}$; (c) $d = 10 \mu\text{m}$, $n_1 = 2.3275$, $n_2 = 1.33$, $\lambda_2 = 300 \text{ nm}$.

The photonic nanojet shown in Fig. 1(c) can be made thinner by increasing the refractive index of the surrounding medium, which is equivalent to decreasing the wavelength of the incident light. This is shown in Fig. 2(a), which visualizes the FDTD-calculated envelope of the sinusoidal steady-state electric field distribution for the parameter set of $d = 5 \mu\text{m}$, $n_1 = 3.5$, $n_2 = 2.0$, and $\lambda_2 = 250 \text{ nm}$. The photonic jet of Fig. 2(a) has a waist of about 160 nm and a length of about 400 nm. In terms of intensity distribution, it has a waist of about 120 nm, smaller than one-half wavelength. We have determined that photonic nanojets similar to that in Fig. 2(a) can be generated using a variety of combinations of d , n_1 , n_2 , and λ_2 provided that n_1/n_2 and d/λ_2 are not changed from the case of Fig. 2(a). This is shown in Fig. 2(b), which visualizes the FDTD-calculated envelope of the sinusoidal steady-state electric field distribution for the parameter set of $d = 6 \mu\text{m}$, $n_1 = 2.3275$, $n_2 = 1.33$, and $\lambda_2 = 300 \text{ nm}$. The photonic jet of Fig. 2(b) has a waist of about 200 nm and a length of about 500 nm. In terms of intensity distribution, it has a waist of about 130 nm, smaller than one-half wavelength. As a final example, Fig. 2(c) illustrates the photonic nanojet produced by the parameter combination $d = 10 \mu\text{m}$, $n_1 = 2.3275$, $n_2 = 1.33$, and $\lambda_2 = 300 \text{ nm}$. All

parameters for this case are the same as for Fig. 2(b) except that the cylinder diameter is increased from 6 μm to 10 μm . Here, the jet has a length of about 1000 nm and a waist of about 200 nm. In terms of intensity distribution, it has a waist of about 140 nm, smaller than one-half wavelength. From these studies, we conclude that the length of the photonic nanojet is effectively controlled by the size of the cylinder whereas the waist of the photonic nanojet is determined by the incident wavelength in the surrounding medium.

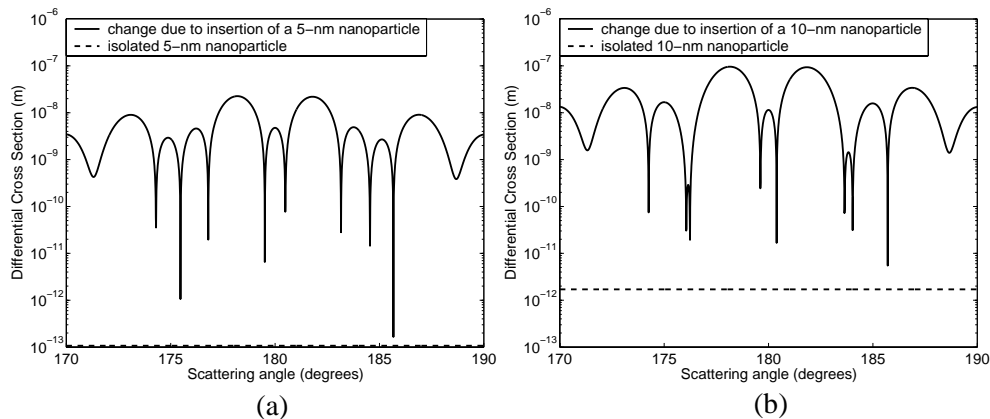


Fig. 3. FDTD numerical results illustrating photonic nanojet enhanced backscattering of light by dielectric nanoparticles. The parameter set of Fig. 2(b) ($d = 6 \mu\text{m}$, $n_1 = 2.3275$, $n_2 = 1.33$, and $\lambda_2 = 300 \text{ nm}$) is assumed. A square, $n = 1.5$ dielectric nanoparticle of side dimension s is inserted at the center of the photonic jet on the surface of the 6- μm cylinder. (a) Absolute value of the change of the differential scattering cross section within $\pm 10^\circ$ of backscatter for $s = 5 \text{ nm}$ compared with the differential scattering cross section of the isolated nanoparticle. (b) Repeated studies of (a) for a nanoparticle of side dimension $s = 10 \text{ nm}$.

3. Photonic nanojet enhanced backscattering of light by nanoparticles

Our further computational investigations of the photonic nanojets illustrated in Figs. 1(c) and 2 indicate that such jets can greatly enhance the effective backscattering of light by nanometer-scale dielectric particles located within the jets. Figures 3 and 4 provide the results of FDTD numerical experiments that illustrate this phenomenon. Here, we consider the case of Fig. 2(b) ($d = 6 \mu\text{m}$, $n_1 = 2.3275$, $n_2 = 1.33$, and $\lambda_2 = 300 \text{ nm}$) with a square, $n = 1.5$ dielectric nanoparticle inserted at the center of the photonic jet on the surface of the 6- μm cylinder. We have adopted double-precision representations for data in our FDTD computer code in order to detect the nanoparticles with fine resolution in our computer experiments.

Figures 3(a) and 3(b) graph the absolute value of the change of the FDTD-calculated differential scattering cross section within $\pm 10^\circ$ of backscatter when a nanoparticle of side dimension $s = 5 \text{ nm}$ and $s = 10 \text{ nm}$, respectively, is inserted at the center of the photonic nanojet. These figures also graph the corresponding differential scattering cross section of the isolated nanoparticle. We see that the effective backscattering cross section of each nanoparticle is enhanced by several orders of magnitude, specifically by $\sim 10^4$ for the 5-nm object and $\sim 10^3$ for the 10-nm object. In addition, the side lobes of the differential cross section near backscattering of the 10-nm object are wider than those of the 5-nm object. This may serve as another indicator for detecting nanoparticles of different sizes.

Figure 4 graphs the backscatter enhancement factor as a function of the size of the nanoparticle. It is apparent that the photonic nanojet created by the much larger 6- μm

cylinder provides a dimensional increase in the effective backscattering cross section of the nanoparticle relative to the case where the nanoparticle is isolated.

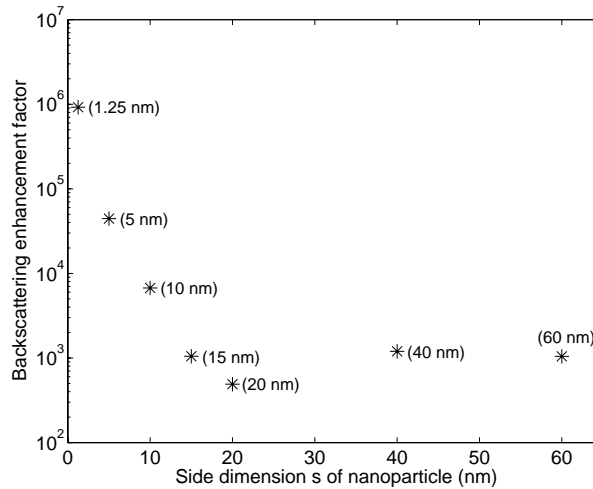


Fig. 4. FDTD numerical results illustrating backscattering enhancement factor as a function of side dimension s of nanoparticles. The parameter set of Fig. 2(b) ($d = 6 \mu\text{m}$, $n_1 = 2.3275$, $n_2 = 1.33$, and $\lambda_2 = 300 \text{ nm}$) is assumed. A square, $n = 1.5$ dielectric nanoparticle of side dimension s is inserted at the center of the photonic jet on the surface of the $6\text{-}\mu\text{m}$ cylinder.

4. Conclusions

In conclusion, we have reported what we believe to be the first evidence of localized nanoscale photonic jets generated at the shadow-side surfaces of micron-scale, circular dielectric cylinders illuminated by a plane wave. These photonic nanojets have waists smaller than the diffraction limit and propagate over several optical wavelengths without significant diffraction. Such nanojets enhance the backscattering of visible light by nanometer-scale dielectric particles located within the jets by several orders of magnitude. Not involving evanescent fields and not requiring mechanical scanning, photonic nanojets may provide a new means to detect and image nanoparticles of size well below the diffraction limit. This could yield a potential novel ultramicroscopy technique using visible light for detecting proteins, viral particles, and even single molecules; and monitoring molecular synthesis and aggregation processes of importance in many areas of biology, chemistry, material sciences, and tissue engineering.

Acknowledgments

This work was supported by National Science Foundation grant BES-0238903.